VNUHCM Journal of Engineering and Technology 2026, 9(2):2902-2911

Open Access Full Text Article

Research Article

Nominal Model Sliding-Mode Repetitive Control of Respiratory Rhythm Generator

Phan Trung Dat[1,2], Truong Cong Toai[1,2], Duong Van Tu[1,2,*]

ABSTRACT

This paper presents a robust control approach for simulating respiratory rhythms using a physical breathing simulator that integrates both respiratory mechanics and blower dynamics. The system models a respiratory rhythm generator driven by a brushless DC motor-based blower, combined with a lumped-parameter artificial lung. To address parameter uncertainties such as time-varying airway resistance and lung compliance arising from physiological variability and modeling inaccuracies, a nominal model sliding mode controller is developed within a repetitive control framework. The proposed scheme consists of two loops: a nominal controller ensuring ideal model tracking, and a plant controller enforcing convergence of the actual output to the nominal response, regardless of parameter mismatches or disturbances. The control algorithm is derived analytically using Lyapunov stability theory and designed to minimize the tracking error of the periodic respiratory volume waveform. To evaluate control system performance, a nonlinear simulation model was constructed incorporating electromechanical dynamics of the blower and physiological variability in lung parameters under time-varying operating condition. Numerical simulations are conducted under three reference inputs with varying tidal volumes and respiratory rates, covering a representative range of breathing conditions. As a result, it demonstrates that the proposed controller reserves high precision across all cases, with normalized root mean square error (NRMSE) consistently exceeding 99.85% and a correlation coefficient of 1.0. The phase trajectory analysis further confirms rapid convergence of tracking error dynamics and bounded steady-state behavior, while the use of a boundary layer saturation function effectively reduces control chattering without degrading tracking performance. This study establishes a high-fidelity simulation platform suitable for ventilator algorithm development, performance testing, and control design under realistic uncertainties. From there, it enables improved robustness evaluation and advanced controller validation in diverse physiological breathing scenarios.

Key words: Nominal model sliding mode, respiratory system, rhythm generator, blower

[1]*Faculty of Mechanical Engineering, Key Laboratory of Digital Control and System Engineering (DCSELab), Ho Chi Minh University of Technology (HCMUT), 268 Ly Thuong Kiet Street, Dien Hong Ward, Ho Chi Minh City, Vietnam*

[2]*Vietnam National University Ho Chi Minh City, Linh Xuan Ward, Ho Chi Minh City, Vietnam*

Correspondence

Duong Van Tu, Faculty of Mechanical Engineering, Key Laboratory of Digital Control and System Engineering (DCSELab), Ho Chi Minh University of Technology (HCMUT), 268 Ly Thuong Kiet Street, Dien Hong Ward, Ho Chi Minh City, Vietnam

Vietnam National University Ho Chi Minh City, Linh Xuan Ward, Ho Chi Minh City, Vietnam

Email: dvtu@hcmut.edu.vn

History

- Received: 09-07-2025
- Revised: 26-09-2025
- Accepted: 23-04-2026
- Published Online: 17-06-2026

DOI : 10.32508/vnuhcmj-et.v9i2.1533

INTRODUCTION

Since the COVID-19 outbreak in late 2019, governments and biomedical researchers have prioritized respiratory medical devices in response to escalating global health concerns[1–8]. This increase of interest has highlighted the acute paucity of ventilatory support equipment in healthcare systems around the world[9]. In addition to supply limitations, another pressing issue involves verifying device performance and ensuring compatibility with individual patients, particularly for mechanical ventilators[10]. The creation and use of breathing simulators, often known as artificial lungs, which mimic human inhalation and/or exhalation patterns, offers a promising way to allay these worries[11]. Importantly, when evaluating ventilators, continuous positive airway pressure (CPAPs), and respiratory therapies, their precision, adaptability, and flexibility make them useful instruments.

In practice, reproducing human breathing profiles that vary across different ages, body conditions,[12] and activity levels remain a considerable challenge[13–15]. Specifically, breathing patterns are highly individualized and depend on factors such as gender, height, body mass, and both physical and psychological health status[16]. Additionally, dynamic factors such as workload intensity can significantly alter respiratory frequency and volume. A research team from Kanazawa University in Japan[17] developed a device to capture and analyze workers' respiratory patterns under physical load, providing essential data for designing a next-generation respiratory rhythm generator. The authors proposed and implemented an electromechanical device that simulates real-time respiratory airflow using a pneumatically actuated cylinder. The device replicated various worker breathing profiles and automatically adjusted for volume discrepancies and airflow measurement errors. The

Cite this article : Trung Dat P, Cong Toai T, Van Tu D. **Nominal Model Sliding-Mode Repetitive Control of Respiratory Rhythm Generator**. *VNUHCM J. Eng. Technol.* 2026; 9(2):2902-2911.

prototype device demonstrated highly reliable results, maintaining a volumetric flow rate deviation of less than 5% between the real and simulated signals. To fully exploit the benefits of such systems, however, it is necessary to collect and catalog a large number of individualized breathing samples, reflecting a wide range of patient profiles across gender, age groups, and working environments [18,19]. Recognizing the educational potential of such simulators, a team from the Czech Republic [20] proposed integrating the active servo lung (ASL) 5000 breathing simulator (Ingmar Medical, USA) with a full-body human patient simulator (ESC, METI, USA). This hybrid setup combines the strengths of both models, enabling in-depth study of respiratory system mechanics, including the influence of lung compliance and airway resistance on ventilation pressure and flow, as well as the effects on gas exchange parameters. Experimental results indicated that a slight change in inspiratory pause flow was the only significant difference between the standalone and integrated configurations. All other parameters, including peak pressure and peak flow rate, were nearly identical, confirming the feasibility of using such an integrated platform for both training and advanced research.

Notwithstanding these advantages, human respiratory behavior with varying physiological and environmental conditions remains a significant challenge in the simulation [21]. Moreover, human breathing patterns are not only individualized but also non-stationary, responding dynamically to factors such as stress, fatigue, exertion level, or underlying pathology [16] . From there, a breathing simulator must be able to adjust parameters such as airway resistance, lung compliance, breathing rate, tidal volume, and inspiratory/expiratory ratios in real time. Furthermore, it should support a wide range of simulated patients, from neonates to adults, under both resting and exertional conditions. In the commercial systems, the ASL 5000 exemplifies state-of-the-art respiratory simulators and has set a high standard for precision and flexibility [22,23]. Essentially, these systems still rely on predefined models and control structures. Additionally, most existing systems focus primarily on the lung-side dynamics, often simplifying or neglecting the actuator-side characteristics, such as the dynamics of flow generation by mechanical blowers or pneumatic pistons. Actually, the actuator's response time, torque, and control accuracy play a significant role in determining the fidelity of the generated respiratory waveform, especially in systems that mimic patient-initiated breathing or deliver high-frequency ventilation.

To address these gaps, this paper develops a physical respiratory rhythm generation model combined with a robust control scheme based on a nominal model sliding-mode framework. First, a respiratory rhythm generator is designed by integrating the dynamic characteristics of a blower with an artificial lung. The blower is driven by a brushless direct current motor (BLDC), which offers higher torque density, faster torque response, greater efficiency, and longer service life compared with brushed direct current motors. The developed apparatus can produce realistic inspiratory-expiratory volume waveforms, serving as a high-fidelity testbed for ventilator control algorithms. Second, this paper introduces a nominal-model-based sliding mode controller in a repetitive control configuration to guarantee accurate tracking of a periodic reference volume signal. A nominal respiratory model is used as an internal reference model, and a sliding mode control (SMC) law is formulated to drive the actual output to follow the reference model output despite uncertainties in airway resistance, lung compliance, and blower parameters. This approach ensures that the tracking error converges to zero within a finite time, even in the presence of parameter mismatches and external disturbances. The proposed controller effectively combines the robustness of SMC with the performance benefits of repetitive cycle-to-cycle learning, without requiring exact knowledge of all system parameters.

In summary, the main contributions of this work are as follows:

- Integrates a physical respiratory rhythm generator model with both detailed respiratory circuit dynamics and the electromechanical behavior of the BLDC-driven blower, capturing actuator-side dynamics often neglected in existing simulators.
- Designed a nominal-model-based sliding mode controller to eliminate adverse effects of parameter uncertainties and unknown disturbances, avoiding fast adaptation issues commonly encountered in MRAC approaches.

SYSTEM MODELING

A simplified dynamic model of the artificial lung, commonly employed in respiratory system devices, can be analogized to an electrical circuit. The transrespiratory pressure P is described by an equation analogous to the voltage equation of such a circuit, expressed as:

$$P(t) = RQ(t) + \frac{V(t)}{C} + P_r, \tag{01}$$

where R and C represent the airway resistance and lung compliance, respectively; P_r denotes residual pressure; the term $Q(t)$ is the volumetric flow rate of air entering the lung, and $V(t)$ the volume of air delivered into the lungs during one inspiratory phase.

The component $RQ(t)$, referred to as the transairway pressure, accounts for pressure loss due to resistive effects within the airways. The term $V(t)/C$ corresponds to the transthoracic pressure required to expand the lung elastically.

In virtue of a blower system actuated by a BLDC motor, the dynamic relationship between the motor's input current and the resulting airflow can be established through electromechanical modeling. The torque generated by the BLDC motor is primarily influenced by the current component along the q-axis, denoted $i_q(t)$.

The electromagnetic torque $T_e(t)$ produced by the BLDC motor is given by:

$$T_e(t) = \frac{3}{2} p K_t i_q(t), \tag{02}$$

where p denotes the number of pole pairs; K_t represents the torque constant, and $i_q(t)$ is the q-axis current component.

The dynamics of the BLDC motor are governed by Newton's second law for rotational systems:

$$J\frac{d\omega(t)}{dt} + b\omega(t) = T_e(t) - T_L(t), \tag{03}$$

where J is the total moment of inertia of the rotor and load, b is the viscous damping coefficient, and $\omega(t)$ is the angular velocity of the motor shaft.

Assuming that the transrespiratory pressure generates a load torque through an effective radius r, cross-sectional area A, and mechanical efficiency η, the resulting torque can be expressed as:

$$T_L(t) = \frac{rA}{\eta} P(t). \tag{04}$$

By using Eqs. (2) and (4), Eq. (3) becomes

$$J\frac{d\omega(t)}{dt} = \frac{3pK_t}{2} i_q(t) - b\omega(t) - K_\tau P(t), \tag{05}$$

where $K_\tau := rA/\eta$.

Assuming the blower airflow rate $Q(t)$ is linearly proportional to the motor's rotational speed, defined as:

$$Q(t) = K_q \omega(t), \tag{06}$$

where K_q is the flow-speed proportionality constant.

By differentiating both sides of Eq. (6) and using Eqs. (1) and (5), the airflow dynamics can be expressed as:

$$\alpha\dot{V}(t) + \beta\dot{V}(t) + \gamma V(t) = u(t) - d, \tag{07}$$

where

$$\alpha := \frac{2J}{3pK_qK_t},\ \beta := \frac{2\left(b + K_qK_\tau R\right)}{3pK_qK_t}, \tag{08}$$

$$\gamma := \frac{2K_\tau}{3pCK_t},\ d := \frac{2K_\tau}{3pK_t} P_r,\ u(t) := i_q(t). \tag{09}$$

Remark 1. $\alpha,\ \beta, \gamma \in R^+$ are uncertainty parameters due to the unknown airway resistance, lung compliance, and mechanical parameters of the blower, with the assumption that $\alpha_m \le \alpha \le \alpha_M, \beta_m \le \beta \le \beta_M$, and $\gamma_m \le \gamma \le \gamma_M$. The term d represents the lump disturbance and unmodeled dynamics, satisfying $|d| \le \bar{d}$, with $\bar{d}$ being a positive unknown constant.

Lemma 1. Let $\theta_m,\ \theta_M \in R^+$ denote the lower and upper bounds of θ, respectively, such that $\theta \in [\theta_m, \theta_M]$. For any value of θ within the interval, the following inequality holds

$$|\theta_a - \theta| \le \frac{\theta_M - \theta_m}{2}, \tag{10}$$

where θ_a is the midpoint of the interval, defined as

$$\theta_a = \frac{\theta_m + \theta_M}{2}. \tag{11}$$

Proof.

Subtracting θ from both sides of Eq. (11), it yields

$$\theta_a - \theta = \frac{\theta_m + \theta_M}{2} - \theta. \tag{12}$$

By introducing an auxiliary term and rearranging the expression, it follows that

$$\theta_a - \theta - \frac{\theta_M - \theta_m}{2} = \theta_m - \theta. \tag{13}$$

Since $\theta \in [\theta_m, \theta_M]$, it follows that $\theta_m \le \theta$. Consequently, the right-hand side of Eq. (13) is non-positive, leading to the following inequality

$$\theta_a - \theta \le \frac{\theta_M - \theta_m}{2}. \tag{14}$$

Similarly, it can be readily shown that

$$\theta_a - \theta \ge -\frac{\theta_M - \theta_m}{2}. \tag{15}$$

By combining Eqs. (14) and (15), the following condition is obtained:

$$|\theta_a - \theta| \le \left|\frac{\theta_M - \theta_m}{2}\right|. \tag{16}$$

Given that $\theta_M > \theta_m$, Eq. (16) simplifies to

$$|\theta_a - \theta| \le \frac{\theta_M - \theta_m}{2}. \tag{17}$$

This completes the proof.

To simulate a cyclical respiratory volume waveform suitable for a respiratory rhythm generator, the variable $V(t)$ in Eq. (7) requires tracking a periodic function that models the breathing cycle's inspiratory and expiratory phases. This formulation captures the essential dynamics of respiratory volume in volume-controlled ventilatory modes. The desired volume waveform $V_d(t)$ is expressed as:

$$V_d(t) = \frac{V_T}{2}\left[1 - cos\left(\frac{2\pi t}{T_c}\right)\right], \tag{18}$$

where T_c is the total duration of one respiratory cycle, involving rhythmic inhalation and exhalation; and V_T is the tidal volume.

CONTROLLER DESIGN

In this paper, a repetitive control process based on nominal model sliding mode control theory is applied to achieve accurate tracking of the periodic reference signal $V_d(t)$. The control block diagram is illustrated in Figure 1. In this structure, the nominal controller is responsible for regulating the nominal output $V_n(t)$ of a nominal model with known parameters to track the reference signal $V_d(t)$, while a plant controller regulates the actual output $V(t)$ to follow the virtual output $V_n(t)$ of the nominal model. This design ensures that the tracking error $e_a(t) := V_d(t) - V(t)$ converges to zero within a finite time, despite the presence of model parameter uncertainties and external disturbances in the system.

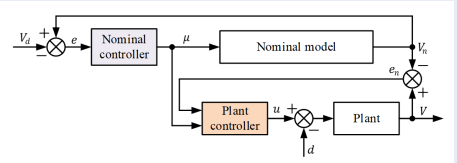

Figure 1: Control block diagram [Source: Authors]

Nominal controller design

Let the nominal model be defined as

$$\alpha_n \ddot{V}_n(t) + \beta_n \dot{V}_n(t) + \gamma_n V_n(t) = \mu(t), \tag{19}$$

where $\alpha_n, \beta_n, \gamma_n \in R^+$ are nominal values of α, β, and γ, respectively, which can be selected appropriately; $\mu(t)$ is the nominal control input; $V_n(t)$ is the nominal air volume.

The nominal tracking error is defined as:

$$e = V_n - V_d. \tag{20}$$

By taking the first and second derivatives of e and rearranging, it yields

$$\begin{cases} \dot{V}_n = \dot{e} + \dot{V}_d \\ \ddot{V}_n = \ddot{e} + \ddot{V}_d \end{cases}. \tag{21}$$

Substituting Eqs. (20) and (21) into Eq. (19) and rearranging, it becomes

$$\ddot{e} + \frac{\beta_n}{\alpha_n}\dot{e} + \frac{\gamma_n}{\alpha_n}e = -\ddot{V}_d - \frac{\beta_n}{\alpha_n}\dot{V}_d - \frac{\gamma_n}{\alpha_n}V_d + \frac{\mu}{\alpha_n}. \tag{22}$$

Theorem 1. The nominal model Eq. (19), with the tracking error defined in Eq. (20), is guaranteed to be asymptotically stable and converge to zero under the following nominal control law:

$$\mu = \alpha_n\left(\ddot{V}_d + \frac{\beta_n}{\alpha_n}\dot{V}_d + \frac{\gamma_n}{\alpha_n}V_d - k_1 e - k_2 \dot{e}\right), \tag{23}$$

where k_1, k_2 denote the positive gains.

Proof.

Substituting Eq. (23) into Eq. (22) yields the dynamic error equation as

$$\ddot{e} + \left(k_2 + \frac{\beta_n}{\alpha_n}\right)\dot{e} + \left(k_1 + \frac{\gamma_n}{\alpha_n}\right)e = 0. \tag{24}$$

To ensure that Eq. (24) satisfies the condition of asymptotic stability with a critically damped response, k_1 and $k_2$can be selected as follows:

$$\begin{cases} k_1 = k_0^2 - \dfrac{\gamma_n}{\alpha_n} \\ k_2 = 2k_0 - \dfrac{\beta_n}{\alpha_n} \end{cases}, \tag{25}$$

where $k_0 > 0$ is the desired pole position.

With the pole placement in Eq. (25) and the control law Eq. (23), the tracking error e converges to zero as $t \to \infty$ according to the Hurwitz stability condition. The proof of Theorem 1 is completed.

Plant controller design

Let $e_n \triangleq V - V_n$ be the model error between the actual plant and the nominal model. The sliding surface can be chosen as:

$$s = \dot{e}_n + \lambda e_n, \tag{26}$$

where $\lambda := \beta_n/\alpha_n$.

Taking the derivative of the sliding surface, it yields

$$\dot{s} = \left(\ddot{V} - \ddot{V}_n\right) + \lambda\left(\dot{V} - \dot{V}_n\right), \tag{27}$$

Theorem 2. The model error e_n between actual plant and the nominal model converges to zero under the following control law:

$$u = -Ks - hsgn(s) + \beta_a \dot{V} + \gamma_a V$$

$$+\alpha_a\left(\frac{\mu}{\alpha_n}-\lambda\dot{V}-\frac{\gamma_n}{\alpha_n}V_n\right), \tag{28}$$

where K is the positive gain,

$$h:=\bar{d}+\frac{\alpha_M-\alpha_m}{2}\left|\frac{\mu}{\alpha_n}-\lambda\dot{V}-\frac{\gamma_n}{\alpha_n}V_n\right|$$

$$+\frac{\beta_M-\beta_m}{2}\left|\dot{V}\right|+\frac{\gamma_M-\gamma_m}{2}|V|,$$

$$\alpha_a:=\frac{\alpha_M+\alpha_m}{2},\beta_a:=\frac{\beta_M+\beta_m}{2},$$

$$\gamma_a:=\frac{\gamma_M+\gamma_m}{2}.$$

Proof.

Let the candidate Lyapunov function be

$$V=\frac{1}{2}\alpha s^2\geq 0. \tag{29}$$

By multiplying Eq. (27) by α and introducing appropriate auxiliary terms, the following expression can be obtained

$$\begin{aligned}\alpha\dot{s}=&\left(\alpha\ddot{V}+\beta\dot{V}+\gamma V\right)-\beta\dot{V}-\gamma V\\&-\frac{\alpha}{\alpha_n}\left(\alpha_n\ddot{V}_n+\beta_n\dot{V}_n+\gamma_nV_n\right)\\&+\frac{\alpha}{\alpha_n}\left(\beta_n\dot{V}_n+\gamma_nV_n\right)+\alpha\lambda\left(\dot{V}-\dot{V}_n\right).\end{aligned} \tag{30}$$

Using Eqs. (7) and (19), Eq. (30) is simplified to

$$\alpha\dot{s}=u-d-\beta\dot{V}-\gamma V-\alpha\left(\frac{\mu}{\alpha_n}-\lambda\dot{V}-\frac{\gamma_n}{\alpha_n}V_n\right). \tag{31}$$

Substituting the control law Eq. (28) into (31), it can be obtained that

$$\begin{aligned}\alpha\dot{s}=&-Ks-h\,sgn(s)\\&+\alpha_a\left(\frac{\mu}{\alpha_n}-\lambda\dot{V}-\frac{\gamma_n}{\alpha_n}V_n\right)+\beta_a\dot{V}\\&+\gamma_aV-d-\beta\dot{V}-\gamma V\\&-\alpha\left(\frac{\mu}{\alpha_n}-\lambda\dot{V}-\frac{\gamma_n}{\alpha_n}V_n\right).\end{aligned} \tag{32}$$

By taking the first-time derivative of Lyapunov function, it yields

$$\dot{V}=\alpha s\dot{s}. \tag{33}$$

By substituting Eq. (32) into Eq. (33), it can be rearranged as follows:

$$\begin{aligned}\dot{V}=&-Ks^2-h|s|\\&+[(\alpha_n-\alpha)\left(\frac{\mu}{\alpha_n}-\lambda\dot{V}-\frac{\gamma_n}{\alpha_n}V_n\right)\\&+(\beta_\alpha-\beta)\dot{V}+(\gamma_\alpha-\gamma)V-d],\end{aligned} \tag{34}$$

which simplifies into the following inequality

$$\begin{aligned}\dot{V}\leq&|s|\left(|\alpha_n-\alpha|\left|\frac{\mu}{\alpha_n}-\lambda\dot{V}-\frac{\gamma_n}{\alpha_n}V_n\right|\right.\\&\left.+|\beta_\alpha-\beta|\left|\dot{V}\right|+|\gamma_\alpha-\gamma||V|+|d|\right)\\&-h|s|.\end{aligned} \tag{35}$$

Using Lemma 1 and the definition in Theorem 2, it can conclude that

$$\begin{aligned}&|d|+|\alpha_a-\alpha|\left|\frac{\mu}{\alpha_n}-\lambda\dot{V}-\frac{\gamma_n}{\alpha_n}V_n\right|\\&+|\beta_a-\beta|\left|\dot{V}\right|+|\gamma_a-\gamma||V|\leq h.\end{aligned} \tag{36}$$

It leads to the condition that

$$\begin{aligned}&|s|\left((|d|+|\alpha_a-\alpha|\left|\frac{\mu}{\alpha_n}-\lambda\dot{V}-\frac{\gamma_n}{\alpha_n}V_n\right|\right.\\&\left.+|\beta_a-\beta|+|\gamma_a-\gamma||V|)-h\right)\leq 0.\end{aligned} \tag{37}$$

From Eq. (37), the inequality (35) becomes $\dot{V}\leq 0$, indicating asymptotic convergence of the tracking error e_n.

The proof of Theorem 2 is completed.

RESULTS AND DISCUSSION

In this numerical study, the airway resistance R, lung compliance C, total moment of inertia J and residual pressure P_r are assumed to be uncertain and time-varying, following the rules:

$$R=R_t\left[1+0.2sin\left(3\pi t\right)\right],$$

$$C=C_t\left[1+0.1sin\left(2\pi t\right)\right],$$

$$J=J_t\left[1+0.2sin\left(\pi t\right)\right],$$

$$P_r=P_{rt}\left[1+0.05sin\left(0.4\pi t\right)\right]. \tag{38}$$

The remaining parameters are known constants. The time variation of the parameters in Eq. (38) results in the time-varying behavior of α,β and γ in the plant described in Eq. (7). The parameters of the nominal model, α_n,β_n and γ_n, are chosen as the average values within the variation ranges of α,β and γ. The control system is simulated over a period of 30 s with a time step of 0.001 s. Additionally, to reduce the chattering phenomenon in the control signal, the sign function $sgn(s)$ in Eq. (28) is replaced by the saturation function $sat(s)$ with a boundary layer $\triangle$. The values of the control parameters as well as the system parameters are detailed in Table 1.

Table 1: System model and control parameters [Source: Authors]

Parameters	Value	Unit
R_t	0.005	$cmH_2O.s.ml^{-1}$
C_t	100	$ml.cmH_2O^{-1}$
P_{rt}	5	cmH_2O
J_t	10^{-6}	$kg.m^2$
p	4	–
K_t	0.2	Nm/A
K_q	1.4	ml/rad
A	0.003	m^2
r	0.03	m
η	0.98	–
b	2×10^{-6}	Nms/rad
k_0	1000	–
K	8×10^{-4}	–
$\triangle$	600	–

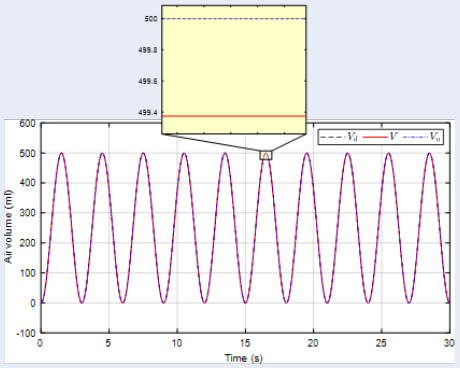

Figure 2: System output response for $V_T = 500\ ml, T_c = 3\ s$ [Source: Authors]

To evaluate the performance of the proposed controller, the breath rhythm generator is configured to control the tidal volume through the lungs to track a reference input signal with the following parameters: $V_T = 500\ ml, T_c = 3\ s$. The system output response is shown in Figure 2, illustrating the relationship between the reference input signal (black dashed line), the output volume of the actual plant (red solid line), and the nominal plant (blue dashed-dot line). Both $V(t)$ and $V_n(t)$ closely follow the reference signal with the same trend and remain consistent throughout the observation period, despite continuous variations in the system parameters and external disturbances.

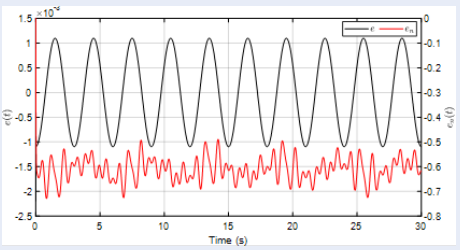

Figure 3: History of $e(t), e_n(t)$ for $V_T = 500\ ml, T_c = 3\ s$ [Source: Authors]

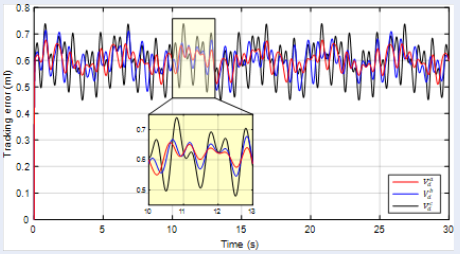

Figure 4: History of $e_a(t)$ with different reference inputs [Source: Authors]

The error $e(t)$ between the output of the nominal plant and the reference signal, as well as the error $e_n(t)$ between the nominal plant and the actual plant, are illustrated more clearly in Figure 3. Due to the nominal control law in Eq. (23), $e(t)$ converges to a very small error range of approximately $\approx \pm 0.0015\ ml$, whereas the magnitude of $e_n(t)$ fluctuates at a higher level, ranging from 0.49 to 0.73 ml. From this figure, it can also be observed that although both errors appear to exhibit periodic characteristics, $e_n(t)$ shows significantly more variations. This is because $e_n(t)$ is directly influenced by the uncertain and time-varying parameters, while $e(t)$ demonstrates a more consistent periodic trend due to its dependence on an ideal model, free of disturbances and with constant parameters. Consequently, the actual tracking error $e_a(t)$ is formed, as shown in Figure 4.

To provide a clearer and more comprehensive evaluation of the proposed controller's performance, the control system is tested with three different reference inputs, $V_d^a(t), V_d^b(t)$ and $V_d^c(t)$, which differ in terms of tidal volume and respiratory cycle, as represented by the following functions:

$$V_d^a(t) = 200\left[1 - cos\left(0.5\pi t\right)\right],$$

$$V_d^b(t) = 250\left[1 - cos\left(\frac{2\pi t}{3}\right)\right],$$

$$V_d^c(t) = 300\left[1 - cos(\pi t)\right]. \quad (39)$$

In Figure 4, the tracking error $e_a(t)$ stays within a relatively narrow range for all reference inputs, mostly between 0.5 and 0.7 ml. Although the specific oscillatory patterns differ slightly depending on the input, the overall error level remains consistent, indicating that the controller maintains stable performance under different operating conditions. The inset highlights this more clearly, showing that the deviations among the three inputs are minimal, indicating that variations in the input waveform have only a minor effect on the tracking behavior.

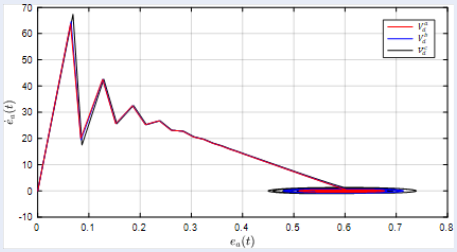

Figure 5: Errorphase trajectory with different reference inputs [Source: Authors]

The corresponding phase portraits in Figure 5 give additional insight into the dynamics between $e_a(t)$ and $\dot{e}_a(t)$. At the start of each run, one can observe larger oscillations, which reflect the controller's effort to correct initial mismatches. Over time, the trajectories shrink into compact elliptical regions, where $\dot{e}_a(t)$ fluctuates around zero while $e_a(t)$ confined within the same narrow band noted earlier. The resemblance of these regions across all reference inputs points to the robustness of the sliding mode control law when the desired volume profile changes.

Figure 6 compares the control signals $u(t)$ across the three scenarios. Consistent with the design, the control inputs remain bounded and exhibit oscillatory behavior characteristic of sliding mode control. Using a saturation function with a boundary layer effectively mitigates high-frequency chattering, resulting in smoother actuation. However, this comes at the cost of a residual steady-state tracking error, as observed in Figure 4. The trade-off between reducing chattering and minimizing error is evident: larger

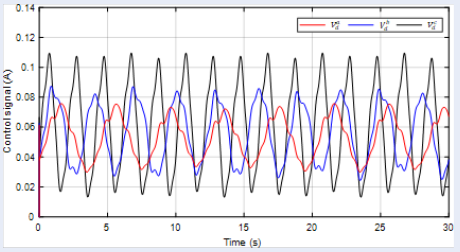

Figure 6: Control history $u(t)$ with different reference inputs [Source: Authors]

boundary layers yield smoother control signals, while smaller ones improve accuracy but at the risk of increased chattering. Across all three reference inputs, the control signals preserve this balance, indicating that the chosen boundary layer parameter achieves a satisfactory compromise between tracking precision and control smoothness.

The normalized root mean square error (NRMSE) and correlation coefficient, R, are used to quantify the similarity between the reference signal and the system output, thereby assessing the control quality. The numerical results are shown in Table 2. The NRMSE values for all three output channels are consistently above 99.85%, indicating excellent agreement between the reference and the measured responses. Moreover, the correlation coefficient R for all outputs reaches 1, implying a perfect linear relationship between the desired and actual signals. These results demonstrate that the controller effectively minimizes both steady-state and dynamic tracking errors, ensuring precise output regulation under the tested conditions. The nearly perfect NRMSE and correlation coefficient values confirm the proposed control strategy's high tracking accuracy and robustness.

Table 2: Performance comparison with different reference inputs [Source: Authors]

Reference	$V_d^a(t)$	$V_d^b(t)$	$V_d^c(t)$
NRMSE (%)	99.85	99.88	99.9
R	1	1	1

CONCLUSION

This study developed a mathematical model of a respiratory rhythm generator incorporating the effects of time-varying airway resistance, lung compliance, inertia, and residual pressure to reflect realistic patient conditions. A sliding mode controller was designed

based on a nominal plant model to achieve robust output tracking despite parameter uncertainties.

Comprehensive numerical simulations were performed under varying operating conditions, including three distinct reference signals representing different tidal volumes and breathing cycles. The proposed controller maintained high tracking accuracy in all scenarios, as quantified by key performance metrics. Specifically, the NRMSE between the system output and the reference signals consistently exceeded 99.85%, while the correlation coefficient reached 1.0 for all cases, indicating a near-perfect linear relationship between the desired and actual outputs. Moreover, the phase trajectory analysis confirmed that the tracking error dynamics rapidly converged to a bounded region, with the steady-state error amplitude remaining within approximately $\pm 0.7\ ml$.

Nevertheless, it should be noted that the current investigation is limited to numerical simulation, and no experimental validation has been performed. Furthermore, the proposed controller relies on a nominal plant model; therefore, tracking can degrade when the practical system departs substantially or changes abruptly. In addition, chattering is mitigated by smoothing the switching action, which necessarily leaves a small residual steady-state error between an inherent smoothness and accuracy trade-off. Moreover, the actuator constraint, comprising current or voltage saturation, fails to be handled within the control law. Notably, in real deployments, sensor noise, actuator delays, and unmodeled nonlinearities are present; thus, the results in this paper should be interpreted as an upper bound on expected performance.

Considering the results obtained and the limitations identified above, future work will focus on implementing the proposed control strategy on a physical prototype to validate its practical effectiveness. In parallel, we will model the nonlinear airway dynamics, including a nonlinear dynamic bronchial constriction and nonlinear compliance, and consider them in the controller design so that the system remains robust even under strong nonlinear behavior. Adaptive or higher-order sliding mode control techniques will be explored to enhance system robustness and tracking accuracy under more challenging operating conditions. Besides, incorporating nonlinear elements into the lung model to improve realism and translational applicability to human lungs enhances physiological fidelity. Furthermore, an experimental scenario with the Spontaneous Breathing Lung Simulator of Michigan Instruments is employed to validate on a physical breathing simulator, which comprises a systematic test matrix spanning R, C, PEEP levels, and controlled leak conditions, with variations in tidal volume and I:E ratio. The metric NRMSE will quantify performance, and correlation alongside clinically relevant indices will be measured. Robustness to sensor noise, measurement delays, and actuator saturation will be rigorously assessed.

LIST OF ABBREVIATIONS

ASL: active servo lung
BLDC: brushless DC
CPAP: continuous positive airway pressure
NRMSE: normalized root mean square error
SMC: sliding mode control

COMPETING INTERESTS

The author(s) declare that they have no competing interests.

AUTHOR CONTRIBUTION

Trung Dat Phan: Writing – original draft, Visualization, Software, Data curation, Investigation.
Cong Toai Truong: Writing – original draft, Visualization, Formal analysis, Data curation, Resources.
Van Tu Duong: Writing – review & editing, Supervision, Methodology, Project administration and Funding acquisition.

ACKNOWLEDGEMENTS

This research is funded by Ho Chi Minh City University of Technology – VNU-HCM under grant number To-CK-2024-05.

REFERENCES

1. Truong CT, Nguyen DK, Tran NQ, et al. Applying the Bilinear Model to Identify the Ventilator's Two Double-Acting Pistons Pump. In: and others, editor. IFMBE Proceedings Springer, Cham; 2024. p. 969–984. Available from: https://doi.org/10.1007/978-3-031-44630-6_77.
2. Nguyen DK, Truong CT, Duong VT, Nguyen HH, Nguyen TT. Model Identification of Two Double-Acting Pistons Pump. Journal of Advanced Marine Engineering and Technology. 2023;47(2):59–65. Available from: https://doi.org/10.5916/jamet.2023.47.2.59.
3. Huynh KH, Truong CT, Phan TD, et al. A Comparative Study on Estimated Methods for Airway Resistance and Lung Compliance in Air Breath Circuit. In: and others, editor. 10th International Conference on the Development of Biomedical Engineering in Vietnam Springer Nature Switzerland: Cham; 2025. p. 324–333. Available from: https://doi.org/10.1007/978-3-031-90194-2_23.
4. Truong CT, Huynh KH, Duong VT, Nguyen HH, Pham LA, Nguyen TT. Model-Free Volume and Pressure-Cycled Control of Automatic Bag Valve Mask Ventilator. AIMS Bioengineering. 2021;8(3):192–207. Available from: https://doi.org/10.3934/bioeng.2021017.
5. Truong CT, Nguyen KD, Duong VT, et al. Model Identification of Two Double-Acting Pistons Pump A NARX Network Approach. In: and others, editor. International Conference on Ubiquitous Robots ; 2023. Available from: https://doi.org/10.1109/UR57808.2023.10202388.

6. Truong CT, Huynh KH, Duong VT, et al. Characteristic of Paddle Squeezing Angle and AMBU Bag Air Volume in Bag Valve Mask Ventilator. In: and others, editor. The 17th International Conference on Intelligent Unmanned Systems; 2021. Available from: https://doi.org/10.48550/arXiv.2109.08019.
7. Truong CT, Huynh KH, Duong VT, Nguyen HH, Pham LA, Nguyen TT. Linear regression model and least square method for experimental identification of AMBU bag in simple ventilator. International Journal of Intelligent Unmanned Systems. 2023;11(3):378–95. Available from: https://doi.org/10.1108/IJIUS-07-2021-0072.
8. Phan TD, Pham LXT, Truong CT, et al. Adaptive Sliding Mode Control for a Blower-Based Breathing Simulator with Unknown and Time-Varying Airway Resistance and Compliance. . In: 10th International Conference on Engineering and Emerging Technologies IEEE: Dubai; 2024. p. 27–28. Available from: https://doi.org/10.1109/ICEET65156.2024.10913788.
9. Olesińska W, Biernatek M, Lachowicz-Wiśniewska S, PiJ. Systematic Review of the Impact of COVID-19 on Healthcare Systems and Society-The Role of Diagnostics and Nutrition in Pandemic Response. Journal of Clinical Medicine. 2025;14(7):2482. Available from: https://doi.org/10.3390/jcm14072482.
10. Gani SM, Mopidevi S, Akul JR, Naru TA, Alayamani DA, Thomas MN, et al. Development of a low-cost portable ventilator system with push mechanism for off-grid and remote patient care. AIP Conference Proceedings. 2025;3291:20002. Available from: https://doi.org/10.1063/5.0269428.
11. Lancmanová A, Bodnár T. Numerical Simulations of Human Respiratory Flows: A Review. Discover Applied Sciences. 2025;7(4):242. Available from: https://doi.org/10.1007/s42452-025-06617-x.
12. Pleil JD, Wallace MAG, Davis MD, Matty CM. The physics of human breathing: flow, timing, volume, and pressure parameters for normal, on-demand, and ventilator respiration. Journal of Breath Research. 2021;15(4):42002. Available from: https://doi.org/10.1088/1752-7163/ac2589.
13. Perricone F, Tartarini L, De Toni L, Rovati L, Mapelli J, Gandolfi D. The road toward a physiological control of artificial respiration: the role of bio-inspired neuronal networks. Frontiers in Neuroscience. 2025;19. Available from: https://doi.org/10.3389/fnins.2025.1638547.
14. Liu M, Duan L. Dynamics and Bifurcation Mechanisms of Respiratory Patterns under Optogenetic Intervention. Nonlinear Dynamics. 2025;113(15):20149–68. Available from: https://doi.org/10.1007/s11071-025-11179-z.
15. Duan L, Chen X, Xia L, et al.. Dynamics and Control of Mixed Bursting in Nonlinear Pre-Bötzinger Complex Systems.; 2024. Available from: https://doi.org/10.1007/978-3-031-44630-6_77.
16. Benchetrit G. Breathing pattern in humans: diversity and individuality. Respiration Physiology. 2000;122(2-3):123–9. Available from: https://doi.org/10.1016/S0034-5687(00)00154-7.
17. Yuasa H, Kumita M, Honda T, Kimura K, Nozaki K, Emi H, et al. Breathing simulator of workers for respirator performance test. Industrial Health. 2015;53(2):124–31. Available from: https://doi.org/10.2486/indhealth.2014-0079.
18. Fens N, Zwinderman AH, van der Schee MP, de Nijs SB, Dijkers E, Roldaan AC, et al. Exhaled breath profiling enables discrimination of chronic obstructive pulmonary disease and asthma. American Journal of Respiratory and Critical Care Medicine. 2009;180(11):1076–82. Available from: https://doi.org/10.1164/rccm.200906-0939oc.
19. Herrera JE, Niehaus WN, Whiteson J, Azola A, Baratta JM, Fleming TK, et al. Multidisciplinary collaborative consensus guidance statement on the assessment and treatment of fatigue in postacute sequelae of SARS-CoV-2 infection (PASC) patients. PM {&}amp; R : The Journal of Injury, Function, and Rehabilitation. 2021;13(9):1027–43. Available from: https://doi.org/10.1002/pmrj.12684.
20. Stránská M, Roubík K, M R. ASL 5000 Lung Model Fails to Simulate Preset Mechanical Parameters During HFJV and Volume Control Ventilation with a Decelerating Flow Waveform in Some Ventilators. 2014;.
21. Acharya D, Das DK. A Systematic Review of Modeling, Clinical Challenges, and Advanced Control Strategies for Artificial Ventilators: From Traditional to Soft Computing Approaches. International Journal of Dynamics and Control. 2024;13(1):8.
22. Hernandez-Garcia L, Aramendía-Vidaurreta V, Bolar DS, et al. Recent Advances in Arterial Spin Labeling: A State-of-the-Art Review. Magnetic Resonance in Medicine. 2022;88(5):2021–42. Available from: https://doi.org/10.1002/mrm.29381.
23. Dexter A, McNinch N, Kaznoch D, Volsko TA. Validating Lung Models Using the ASL 5000 Breathing Simulator. Simulation in Healthcare : Journal of the Society for Simulation in Healthcare. 2018;13(2):117–23. Available from: https://doi.org/10.1097/SIH.0000000000000277.

VNUHCM Journal of Engineering and Technology 2026, 9(2):2902-2911

Open Access Full Text Article

Bài nghiên cứu

Thuật Toán Điều Khiển Lặp Lại Trượt dựa trên Mô Hình Chuẩn cho Máy Tạo Nhịp Thở

Phan Trung Đạt[1,2], Trương Công Toại[1,2], Dương Văn Tú[1,2,*]

Use your smartphone to scan this QR code and download this article

TÓM TẮT

Bài báo này trình bày một phương pháp điều khiển bền vững nhằm mô phỏng nhịp thở sinh lý bằng cách sử dụng một thiết bị mô phỏng nhịp thở vật lý tích hợp cả cơ học hô hấp và động học của bộ tạo lưu lượng. Hệ thống được mô hình hóa như một bộ tạo nhịp thở sử dụng quạt thổi điều khiển bằng động cơ không chổi than (BLDC), kết hợp với một mô hình phổi nhân tạo tham số tập trung. Để đối phó với sự không chắc chắn của các tham số như sức cản đường thở và độ đàn hồi phổi thay đổi theo thời gian, bài báo đề xuất một bộ điều khiển trượt dựa trên mô hình danh định (nominal model sliding mode controller – SMC) trong cấu trúc điều khiển lặp lại. Hệ thống điều khiển bao gồm hai vòng: bộ điều khiển mô hình danh định đảm bảo theo dõi đầu ra lý tưởng, và bộ điều khiển hệ thực thi buộc đầu ra thực tế hội tụ về đầu ra mô hình, bất chấp sai lệch tham số hoặc nhiễu bên ngoài. Thuật toán điều khiển được thiết kế dựa trên lý thuyết ổn định Lyapunov nhằm giảm thiểu sai số theo dõi của tín hiệu thể tích hô hấp dạng tuần hoàn. Để đánh giá hiệu suất hệ thống, một mô hình mô phỏng phi tuyến được xây dựng bao gồm cả động học điện cơ của bộ tạo lưu lượng và biến thiên sinh lý trong các thông số phổi. Các mô phỏng số được thực hiện với ba tín hiệu tham chiếu khác nhau, thay đổi thể tích khí lưu thông và chu kỳ hô hấp, phản ánh phổ biến các kiểu thở thực tế. Kết quả cho thấy bộ điều khiển đề xuất duy trì độ chính xác rất cao trong các trường hợp đánh giá, với sai số bình phương trung bình chuẩn hóa là 99,85% và hệ số tương quan đạt 1,0. Phân tích quỹ đạo pha xác nhận khả năng hội tụ nhanh của sai số theo dõi và hành vi ổn định trong trạng thái dừng, trong khi việc sử dụng hàm bão hòa với lớp biên giúp giảm hiện tượng dao động điều khiển (chattering). Nghiên cứu này thiết lập một nền tảng mô phỏng độ trung thực cao, phù hợp cho việc phát triển thuật toán điều khiển máy thở, đánh giá hiệu suất và thiết kế bộ điều khiển trong điều kiện các thông số hệ thống không chắc chắn xác định.

Từ khoá: trượt dựa trên mô hình mẫu, máy tạo nhịp, hệ thống thông khí, quạt thổi

[1]*Khoa Cơ Khí, Trường Đại học Bách Khoa TP.HCM*

[2]*Đại học Quốc gia Thành phố Hồ Chí Minh*

Liên hệ

Dương Văn Tú, Khoa Cơ Khí, Trường Đại học Bách Khoa TP.HCM

Đại học Quốc gia Thành phố Hồ Chí Minh

Email: dvtu@hcmut.edu.vn

Lịch sử

- Ngày nhận: 09-07-2025
- Ngày sửa đổi: 26-09-2025
- Ngày chấp nhận: 23-04-2026
- Ngày đăng: 17-06-2026

DOI : 10.32508/vnuhcmj-et.v9i2.1533

Check for updates

Trích dẫn bài báo này: Đạt P T, Toại T C, Tú D V. **Thuật Toán Điều Khiển Lặp Lại Trượt dựa trên Mô Hình Chuẩn cho Máy Tạo Nhịp Thở**. *VNUHCM J. Eng. Technol.* 2026; 9(2):2902-2911.